Research Paper
J. Astron. Space Sci. 32(4), 349-355 (2015)
http://dx.doi.org/10.5140/JASS.2015.32.4.349

JASS Journal of Astronomy and Space Sciences

Magnitude Standardization Procedure for OWL-Net Optical Observations of LEO Satellites

Dong-Goo Roh[1†], Jin Choi[1,2], Jung Hyun Jo[1,2], Hong-Suh Yim[1], Sun-Youp Park[1], Maru Park[1,3], Young-Jun Choi[1], Young-Ho Bae[1], Young-Sik Park[1], Hyun-Jung Jang[1], Sungki Cho[1,2], Ji-Hye Kim[1], Jang-Hyun Park[1]

[1]Korea Astronomy and Space Science Institute, Daejeon 34055, Korea
[2]Korea University of Science and Technology, Daejeon 34113, Korea
[3]Chungbuk National University, Cheongju 28644, Korea

As a governmentally approved domestic entity for Space Situational Awareness, Korea Astronomy and Space Science Institute (KASI) is developing and operating an optical telescopes system, Optical Wide-field PatroL (OWL) Network. During the test phase of this system, it is necessary to determine the range of brightness of the observable satellites. We have defined standard magnitude for Low Earth Orbit (LEO) satellites to calibrate their luminosity in terms of standard parameters such as distance, phase angle, and angular rate. In this work, we report the optical brightness range of five LEO Satellites using OWL-Net.

Keywords: OWL-Net, LEO satellites, photometry, magnitude standardization, phase angle, range

1. INTRODUCTION

Due to the progress in space development, the possibility of threats to space assets by other space objects is growing. As a space club member, it is necessary to maintain a space surveillance program for purposes of national interest. In 2010, the Republic of Korea initiated the Optical Wide-field patroL Network (OWL-Net), an optical space surveillance infrastructure (Park et al. 2012). It was intended that OWL-Net would include five identical telescopes, cameras, and site operating systems. Five observatory sites were selected to satisfy the requirement of longitudinal separation. OWL telescopes have a 0.5 m aperture and 1.1° × 1.1° field of view. The network adopts a chopper system to track moving objects within an image into multiple streaks; therefore, enabling multiple observation points for a single target with one exposure (Park et al. 2014). Based on this capability, one of the main goals for OWL was to track Low Earth Orbit (LEO) satellites and to maintain their ephemeris, in addition to tracking Geostationary Earth Orbit (GEO) satellites and maintaining of their ephemeris (Park et al. 2015; Son et al. 2015a, b).

From the early space era, optical observation systems have been used to track satellites in order to estimate their orbits and physical characteristics (Veis 1963). Moreover, satellite brightness information can be used to estimate the size of target satellites. Size Estimation Models (SEM) are used to analyze satellite brightness; for example, the Optical Size Estimation Model (OSEM), which is applied with a Lambertian spherical phase function based on the empirically derived SEM of the National Aeronautics and Space Administration (NASA; Bohannon & Young 1993). However, the capabilities of satellite brightness models are limited by a lack of data regarding satellites' material, shape, and size, which impact on the optical brightness by controlling surface material composition, albedo, and

Received Nov 12, 2015 **Revised** Nov 24, 2015 **Accepted** Nov 26, 2015
†**Corresponding Author**
E-mail: rrdong9@kasi.re.kr, ORCID: 0000-0001-6104-4304
Tel: +82-42-865-2088, Fax: +82-42-861-5610

scattering functions of an object's surfaces (Africano et al. 2000; Bruski et al. 2012).

Ackermann et al. (2003) observed the optical signatures of small LEO satellites and analyzed the various search strategies for identifying these objects. However, these satellite brightness observations have tended to target GEO satellites. The brightness of GEO satellites was studied by Payne et al. (2007), who performed color observations using Johnson B and R filters, and analyzed short- and long-term variations in satellite brightness. Seo et al. (2013) attempted to measure the brightness of Korean GEO Communication, Ocean and Meteorological Satellites (COMS) using the ray-tracing method. Congnion (2013) observed five GEO satellites and compared brightness results using the Lambertian method and the empirical method at large phase angles.

Previous satellite observation studies were performed using small aperture telescopes with various lower limiting magnitudes and spatial resolutions, and with no standard value of magnitude based on absolute magnitudes of stellar brightness. Photometric results of satellite magnitude can differ according to observational conditions at each site, even when using the same optical systems. Therefore, the standardization of satellite brightness quantification has become necessary, and in particular, there is a need to define the brightness of LEO satellites using photometric results standardized across observation sites and telescopes.

In this study, we performed photometric observations of five LEO satellites using the OWL-Net telescope, with data collected from the Mongolian station. These observation results were used to define an absolute magnitude for LEO satellites.

2. METHODLOGY

We produced three magnitude types that depended on the progress of data processing: apparent instrumental magnitude, normalized magnitude, and airmass corrected magnitude. The magnitude derived in the final step of data processing was taken as the standard magnitude for LEO satellites. We used optical observation data of five LEO satellites: COSMOS 1455, COSMOS 1726, COSMOS 2428, Gravity Probe B, and SEASAT 1 (Table 1).

2.1 Instrumental Magnitude

Apparent instrumental magnitude was acquired from the pipeline of OWL data reduction (Park et al. 2013). The OWL system uses the Source Extractor (Bertin & Arnouts 1996) for photometry, and can efficiently locate any point in an image that is brighter than a user-specified noise level over the sky background. The system then outputs the coordinates, brightness, error, and shape parameters of the bright sources identified. When a moving object is exposed to the OWL-Net detector system, it results in a group of multiple aligned streaks that are generated by the chopper system.

2.2 Exposure Time Normalization

During the exposure, chopper blades repeatedly close and open the Charge Coupled Device (CCD) window. Each streak can have various exposure times (in milliseconds), while the exposure time of the image is up to several seconds. Correcting for the exposure time was the first step in normalizing magnitude. Exposure times of streaklets were normalized to 1 s, and streaklet brightness was then normalized based on this exposure time.

2.3 Range Normalization

When precise observation times of streaklets from LEO satellites are obtained, we are able to calculate the range

Table 1. Physical characteristics and observational data for target LEO[a] satellites

	COSMOS 1455	COSMOS 1726	COSMOS 2428	Gravity Probe B	SEASAT 1
Observation Day	20141101, 20141104	20141101, 20141102, 20141103, 20141105	20150210, 20150211, 20150212, 20150213	20141101, 20141102, 20141103, 20141104, 20141105, 20151106	20141121, 20141123, 20141127
Size (m)	1.3×1.3×3.2	1.3×1.3×3.2	1.4×1.4×4.46	2.64×2.64×6.43	1.5×1.5×21
Shape	Cylinder and wing	Cylinder and wing	Cylinder and wing	Cylinder and wing	Cylinder and wing
Perigee (km)	519.5	508.5	851.5	640.8	753.0
Apogee (km)	547.9	530.9	864.3	645.3	756.8
Operational	×	×	○	×	×

a. LEO = Low Earth Orbit

between the LEO satellite and the telescope, which varies as a function of time, using the Analytical Graphics Inc. (AGI) Satellite Tool Kit (STK) and LEO Two Line Elements (TLE) data. We assumed that the range-normalized magnitude was equivalent to the stellar absolute magnitude, and adopted 1,000 km as the standard range. Thus, the brightness of the satellite could be normalized using the expression:

$$F_{r\_cor} = F_i \times (\frac{r}{1000})^2 \quad (1)$$

where r is the range of a satellite in km. Generally, TLE have uncertainties of ~1–2 km in the range direction (Vallado et al. 2013); therefore, the errors in normalized brightness correspond to this uncertainty.

2.4 Phase Angle Normalization

Satellite brightness can be analyzed using the Lambertian spherical phase angle correction (Whitmell 1907). Detailed information on the shape, material, and orientation for each target are required to estimate precise brightness variations; however, we focused on describing variations in satellite brightness without using these data (i.e., we assumed that all observed LEO satellites have a spherical shape and are made of the same and homogenous materials). Environmental conditions were corrected using the Lambertian spherical model (Cognion 2013).

To normalize reflection environmental conditions for satellite brightness, we considered phase angle and range. The level of sunlight reflected by a satellite varies as a function of the phase angles between the Sun, satellites, and telescope. Phase angle was calculated using STK and TLE data, with a Lambertian spherical phase correction performed using the expression:

$$F_{PA\_cor} = F_i \times \frac{2}{3} \times (\frac{\sin(\varphi)+(\pi-\varphi)\cos(\varphi)}{\pi}) \quad (2)$$

where φ is the phase angle in radians.

2.5 Airmass Correction

Reflected light from LEO satellites is attenuated as it passes through the Earth's atmosphere owing to scattering and absorption. To correct for the extinction effect of the atmosphere, we independently performed astronomical standard photometry for calibration using a catalog based on Landolt (1992). We obtained observational data from a single calibration night using Johnson B, V, R, and I filters. In addition to allowing the standardization of stellar brightness, this approach allows for the analysis of optical and site atmosphere characteristics (e.g., limit magnitude and sky brightness). However, due to differences in sky conditions on different observation nights, there is no guarantee that atmospheric extinction values are representative of actual atmospheric conditions at the time of the satellite observation.

Optical observation data was obtained from the first OWL-Net observatory, located in Mongolia. We used the R filter for the whole observation. Atmospheric extinction was corrected using the expression:

$$Mag_{air\_cor} = Mag_i - (k_R \times X + Mag_{ZP}) \quad (3)$$

where k_R is the coefficient of atmospheric extinction for the R filter (0.2625 ± 0.1340), Mag_{ZP} is the zero point of magnitude for the R filter (4.1260 ± 0.2147), and X is the airmass value for the observed satellite.

3. RESULTS

For the COSMOS 1455 satellite, variations in apparent magnitude fell following the 4-step satellite brightness correction procedure (Fig. 1). Variations in standard absolute magnitude were within one order of magnitude, and we found that the range correction had the dominant impact. In contrast, the phase angle correction made no significant improvement to the variation in satellite brightness (Fig. 2). Despite correcting for phase angle and range, we still observed variations in the brightness of COSMOS 1455, reflecting the effects of shape, albedo, and satellite attitude, which we had originally excluded from consideration. We also observed variations in the magnitudes of images with the same exposure time. Optical instability of images (e.g., the vignetting phenomenon) may have occurred because of the absence of a flat correction in the OWL-Net data reduction pipeline.

Variations in magnitude for the COSMOS 1726 satellite also fell following the magnitude correction process, and again the impact of the range correction was dominant (Figs. 3 and 4). In contrast, the standard absolute magnitudes of the COSMOS 2428 satellite (Figs. 5 and 6) and the Gravity Probe B satellite (Figs. 7 and 8) varied by more than three orders of magnitudes, despite the application of the magnitude correction process. For Gravity Probe B, magnitude differences were also observed among streaklets in same exposure images. Finally, the SEASAT 1 satellite showed more than four orders of magnitude variation in standard absolute magnitude, and differences in the brightness of streaklets were also observed (Figs. 9 and 10).

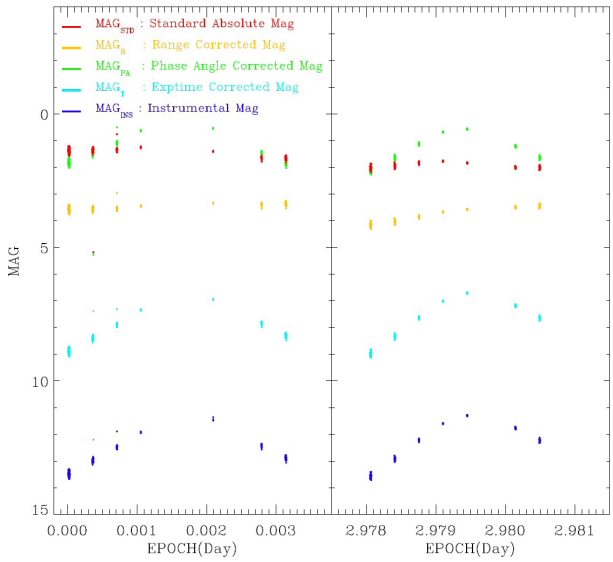

Fig. 1. Magnitudes for the COSMOS 1455 satellite generated from each step in the standardization procedure.

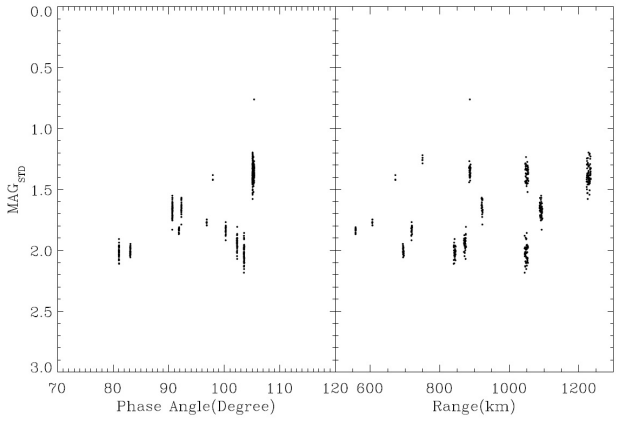

Fig. 2. Standard absolute magnitude vs. Sun phase angle and range to the COSMOS 1455 satellite from the observation site.

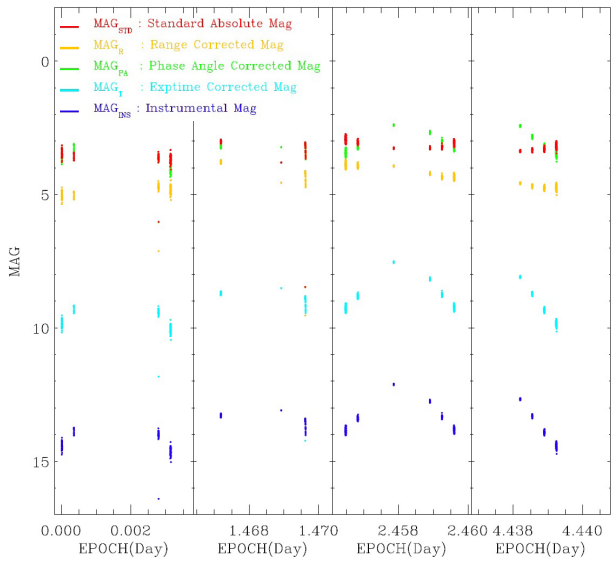

Fig. 3. Magnitudes for the COSMOS 1726 satellite generated from each step in the standardization procedure.

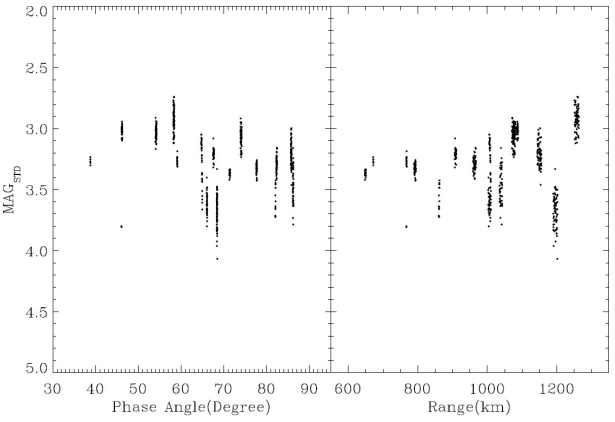

Fig. 4. Standard absolute magnitude vs. Sun phase angle and range to the COSMOS 1726 satellite from the observation site.

As discussed, these variations in magnitude likely reflected the shape, albedo, and attitude of the satellites.

4. DISCUSSION AND CONCLUSIONS

We defined the standardized magnitude of LEO satellite brightness, and normalized the brightness of streaklets made by LEO satellites using a 1 s exposure, zero phase angle, and 1,000 km range. The final magnitude was corrected for the atmospheric extinction effect. Observational data from the OWL-Net was used to apply our magnitude standardization procedure; as a result, we obtained standardized magnitude curves for the brightness of five LEO satellites. However, despite our standardization, we still observed variations in magnitude, with variations occurring over both the short- and long-term.

Short-term variations occurred with single exposures, and were consistent with those observed in the original instrumental magnitude; therefore, our magnitude standardization procedure failed to purge short-term variations in the observation data. We found that the dynamic range of the instrument magnitude in a single exposure could reach up to two orders of magnitudes in worst-case scenarios (Figs. 1, 3, 5, 7, and 9). Owing to the short exposure time (1 sec), the satellite attitude, Sun phase angle, and satellite shape can be discounted as possible causes of these variation. The exposure time for each streaklet was less than 20 msec; nevertheless, the OWL data processing pipeline designed to produce metric

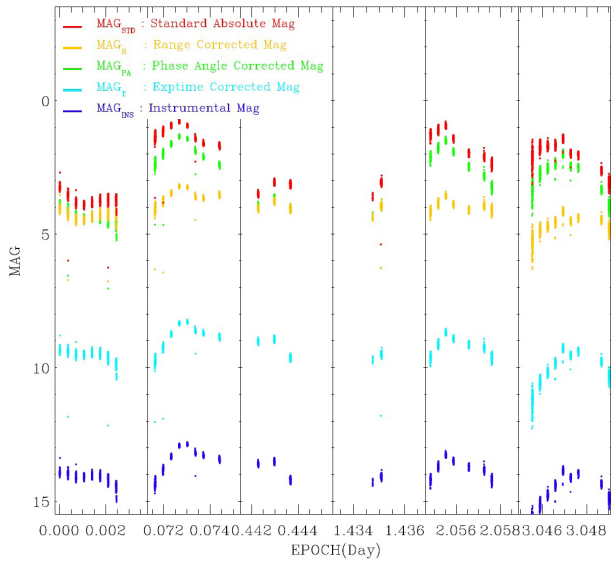

Fig. 5. Magnitudes for the COSMOS 2428 satellite generated from each step in the standardization procedure.

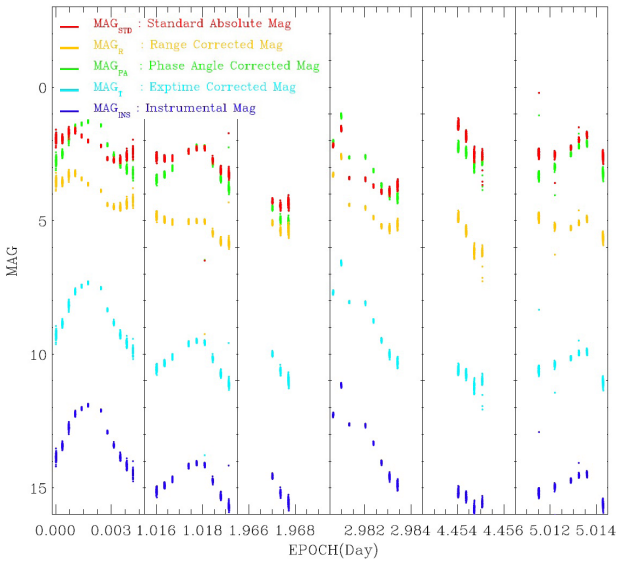

Fig. 7. Magnitudes for the Gravity Probe B satellite generated from each step in the standardization procedure.

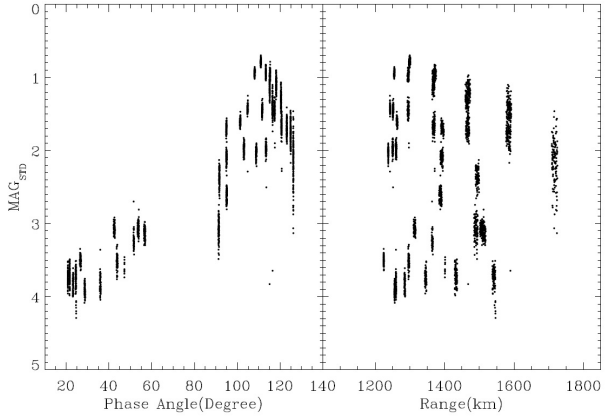

Fig. 6. Standard absolute magnitude vs. Sun phase angle and range to the COSMOS 2428 satellite from the observation site.

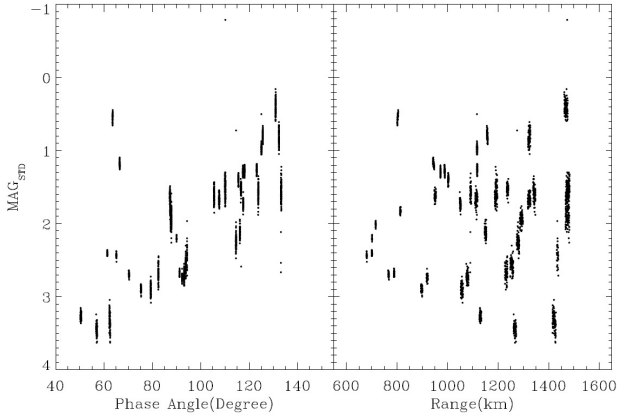

Fig. 8. Standard absolute magnitude vs. Sun phase angle and range to the Gravity Probe B satellite from the observation site.

data for orbital ephemeris based on the astrometric World Coordinate System (WCS). Thus, neither flat correction of the CCD image or correction of optical vignette were applied to the original CCD optical observation images. Without these corrections, the brightness of each streaklet can be diminished by its position within the image; therefore, improvements to the OWL data reduction pipeline, including the precise preprocessing of images, are needed for the correction of short-term brightness variations.

Long-term magnitude variations were removed by our magnitude standardization procedures for COSMOS 1455 and COSMOS 1726. However, the standardized magnitude of the other three satellites showed inconsistent behavior when compared with the two successfully standardized outcomes. We concluded that the shape and attitude of satellites, which we removed from consideration, gave rise to these variations. Among the four procedures within our magnitude standardization, the range correction played the most significant role (Figs. 1 and 3). Though the standardized magnitude did not show a flat response (Figs. 5, 7, and 9), the brightness correction by the range normalization was critical in flattening the magnitude variations.

ACKNOWLEDGMENTS

This work was supported by the National Agenda Project "Development of Electro-optic Space Surveillance System" funded by the Korea Research Council of Fundamental

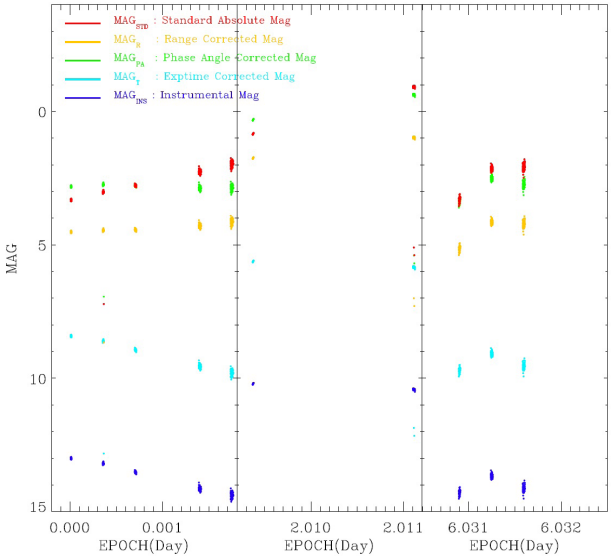

Fig. 9. Magnitudes for the SEASAT 1 satellite generated from each step in the standardization procedure.

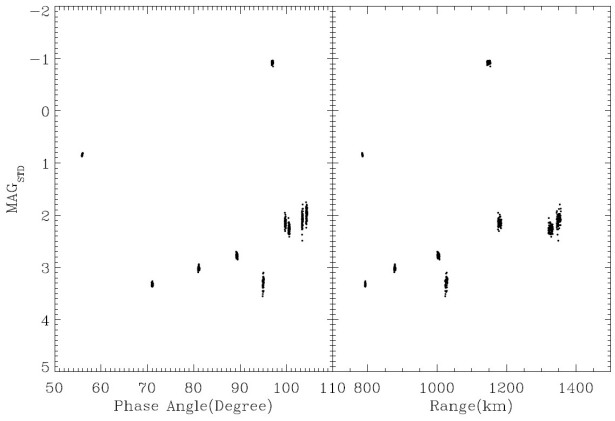

Fig. 10. Standard absolute magnitude vs. Sun phase angle and range to the SEASAT 1 satellite from the observation site.

Science & Technology (KRCF) and the Korean Astronomy and Space Science Institute (KASI).

REFERENCES

Ackermann MR, McGraw JT, Martin JB, Zimmer PC, Blind Search for Micro Satellites in LEO: Optical Signatures and Search Strategies. Proceedings of the 2003 AMOS Conference, Hawaii, United States, 7-13 Sep 2003.

Africano J, Schildknecht T, Matney M, Kervin P, Stansbery E, et al., A Geosynchronous Orbit Search Strategy, Space Debris 2, 357-369 (2000). http://dx.doi.org/10.1023/B:SDEB.0000030025.04930.08

Bertin E, Arnouts S, SExtractor: Software for source extraction, Astron. Astrophys. Suppl. Series 117, 393-404 (1996). http://dx.doi.org/10.1051/aas:1996164

Bohannon GE, Young N, Debris Size Estimation Using Average RCS Measurements, XonTech, Inc. Report, 930781-BE-2247 (1993).

Bruski S, Harms SR, Jones MP, Thomas N, Dahlke SR, Determination of Satellite Characteristics through Visible Light Intensity Analysis, Proceedings of the 2012 AMOS Conference, Hawaii, United States, 11-14 Sep 2012.

Cognion R, Observations and Modeling of GEO Satellites at Large Phase Angles, Proceedings of the 2013 AMOS Conference, Hawaii, United States, 10-13 Sep 2013.

Landolt AU, UBVRI photometric standard stars in the magnitude range 11.5-16.0 around the celestial equator, Astron. J. 104, 340-371 (1992). http://dx.doi.org/10.1086/116242

Park JH, Choi YJ, Jo JH, Moon HK, Yim HS, et al., Korean space Situational Awareness Program: OWL Network, Proceedings of the 2012 AMOS Conference, Hawaii, United States, 11-14 Sep 2012.

Park JH, Choi YJ, Jo JH, Moon HK, Yim HS, et al., Proto-Type Development of Optical Wide-field Patrol Network and Test Observation, Proceedings of the 2012 AMOS Conference, Hawaii, United States, 15-18 Sep 2014.

Park SY, Keum KH, Lee SW, Jin H, Park YS, et al., Development of a Data Reduction algorithm for Optical Wide Field Patrol, J. Astron. Space Sci. 30, 193-206 (2013). http://dx.doi.org/10.5140/JASS.2013.30.3.193

Park SY, Choi J, Jo JH, Son JY, Park YS, et al., Development of a Reduction Algorithm of GEO Satellite Optical Observation Data for Optical Wide Field Patrol (OWL), J. Astron. Space Sci. 32, 201-207 (2015). http://dx.doi.org/10.5140/JASS.2015.32.3.201

Payne TE, Gregory SA, Martin JB, Tombasco J, Luu K, et al., Satellite Monitoring, Change Detection, and Characterization Using Non-Resolved Electro-Optical Data From a Small Aperture Telescope, Proceedings of the 2007 AMOS Conference, Hawaii, United States, 12-14 Sep 2007.

Seo H, Jin H, Song Y, Lee Y, Oh Y, The Photometric Brightness Variation of Geostationary Orbit Satellite, J. Astron. Space Sci. 30, 179-185 (2013). http://dx.doi.org/10.5140/JASS.2013.30.3.179

Son JY, Jo JH, Choi J, Optical Orbit Determination of a Geosynchronous Earth Orbit Satellite Effected by Baseline Distances between Various Ground-based Tracking Stations I: COMS simulation case, J. Astron. Space Sci. 32, 221-228 (2015a). http://dx.doi.org/10.5140/JASS.2015.32.3.221

Son JY, Jo JH, Choi J, Kim BY, Yoon JN, et al., Optical Orbit

Determination of a Geosynchronous Earth Orbit Satellite Effected by Baseline Distances between Various Ground-based Tracking Stations II: COMS Case with Analysis of Actual Observation Data, J. Astron. Space Sci. 32, 229-235 (2015b). http://dx.doi.org/10.5140/JASS.2015.32.3.229

Vallado DA, Virgili BB, Flohrer T, Improved SSA Through Orbit Determination of Two-Line Elements Sets, Proceedings of the 6th European Conference on Space Debris, Darmstadt, Germany, 22-25 Apr 2013.

Veis G, Optical tracking of artificial satellites. Space Sci. Rev. 2, 250–296 (1963). http://dx.doi.org/10.1007/BF00216781

Whitmell CT, Brightness of a Planet, The Observatory 30, 96-100 (1907).